

# We are IntechOpen, the world's leading publisher of Open Access books Built by scientists, for scientists

6,900

Open access books available

185,000

International authors and editors

200M

Downloads

Our authors are among the

154

Countries delivered to

TOP 1%

most cited scientists

12.2%

Contributors from top 500 universities



WEB OF SCIENCE™

Selection of our books indexed in the Book Citation Index  
in Web of Science™ Core Collection (BKCI)

Interested in publishing with us?  
Contact [book.department@intechopen.com](mailto:book.department@intechopen.com)

Numbers displayed above are based on latest data collected.  
For more information visit [www.intechopen.com](http://www.intechopen.com)



---

# Utilization of Composites and Nanocomposites Based on Natural Rubber and Ceramic Nanoparticles as Control Agents for *Leishmania braziliensis*

---

Aldo Eloizo Job, Alexandre Fioravante de Siqueira,  
Caroline Silva Danna, Felipe Silva Bellucci,  
Flávio Camargo Cabrera and  
Leandra Ernst Kerche Silva

Additional information is available at the end of the chapter

<http://dx.doi.org/10.5772/57211>

---

## 1. Introduction

Nanoscience and Nanotechnology are revolutionizing the world of science and technology, bringing high expectations for technological innovation and the development of areas, such as: aerospace, agribusiness, defense, energy, environment, nanodevices, nanosensors, textiles, biotechnology and health. As part of its application to the health sciences, one of the priority targets are negligible diseases such as Leishmaniasis. In this context, the main objective of this chapter is to show the potential of some classes of ceramic nanoparticles and magnetic and ferroelectric nanocomposites based on natural rubber to modulate the growth of parasite colony of *Leishmania braziliensis* (LB) and to evaluate the toxicity of these materials against mammal cells.

### 1.1. Nanoscience and nanotechnology applied to neglected diseases

Materials with sizes ranging between  $1 \times 10^{-9}$  m and  $100 \times 10^{-9}$  m are called nanomaterials regardless of their nature, whether ceramic, polymer, metal or composite. When a material has dimensions on the nanometric scale, its surface properties and volume are differentiated in relation to material properties at a higher dimensional scale. These differences occur because the surface/volume ratio or high aspect ratios are not linear for different dimensional scales and this is in part responsible for the differentiated properties presented by nonascale materials. These

differentiated properties can be transferred to other materials by the insertion of the nanomaterials in a matrix of a different nature and nanometric scale not generating a nanocomposite material [1, 2]. In general, the choice of polymer as a matrix or continuous phase is preferable since most have appreciable thermal and mechanical properties. Other properties must also be taken into account, such as hydrophobic/hydrophilic balance, chemical stability and biocompatibility. The nanometric component, generally inorganic, known as the dispersed phase, can provide a higher mechanical, thermal stability and also biological properties [3].

Multidisciplinary researches involving nanoscience, nanotechnology, materials science and engineering, biotechnology and health sciences have gained great strength in recent decades, aiming to increase the number of tools for addressing problems [4]. Each day new materials and methodologies are tested in fighting diseases such as cancer and diseases neglected by the pharmaceutical industry, for example, malaria, leishmaniasis and Chagas' disease. As a result of this innovation, nanocomposites and composites based in natural rubber filled with ceramic particle and nanoparticles can be used in biological applications, aiming at development of devices such as intelligent bandages or agents of control and reduction of parasitic colonies [5].

### 1.2. *Leishmania braziliensis*

Leishmaniasis is an endemic and parasitic infection caused by the *Leishmania* genus protozoa. Approximately 1.5 million people were affected by cutaneous leishmaniasis, which reaches 88 countries and has compulsory notification in only 30 of them. Presents itself throughout the Americas and Brazil is the country that has the highest prevalence of cases. Leishmaniasis is a typically tropical disease from Trypanosomatidae family, affecting the skin (cutaneous leishmaniasis, caused by *Leishmania braziliensis* protozoans) or viscera (visceral leishmaniasis, caused by *Leishmania donovani* protozoans), transmitted by the bite of the vector, a phlebotomine sand fly popularly known as "straw mosquito", which utilizes both animals and humans as host [6, 7].

Protozoans of *Leishmania* genus are unicellular, eukaryotic, heterotrophic, with asexual reproduction by binary fission, and feed via uptake of non-self-generated food. Within the human body, *Leishmania* protozoans feed of proteins present intracellularly or in blood plasma, and reproduce only within macrophages or similar cells of the immune system [6, 7].

### 1.3. Ceramic materials

Ceramic materials (in general, oxides, carbides or nitrides) are inorganic, non-metallic substances consisting of metallic and non-metallic elements connected together by covalent and/or ionic bonds. This class of materials displays a set of distinguished physical and chemical properties such as high mechanical strength, high hardness, low tenacity, low thermal and electrical conductivity, high melting point, among others. As a result of the variety of properties that ceramic materials exhibit, these materials have various industrial applications as, for example, bricks, crockery, refractory glass mortars, magnetic materials, electronic devices, fibers, abrasives and aerospace components.

Ceramic phases preparation processes can be classified primarily in chemical and physical routes, and the appropriate processing route selection depends on several aspects associated with the desired final product characteristics, such as desired dimensional scale, final product purity degree, ceramic phase complexity, amount of obtained material, desired physical and chemical properties and cost of the final product. Among several ceramic phases currently known, investigated and used, those with magnetic and ceramic properties with ferroelectric properties can be highlighted, e.g. ferrite with inverse spinel type structure and niobate potassium strontium with tetragonal tungsten bronze structure [8, 9].

### 1.3.1. Inverse spinel structure and the nickel-zinc ferrite

Among the materials with inverse spinel type structure, is highlighted the Ni-Zn ferrite paramagnetic or superparamagnetic ceramic phase, with cubic symmetry and space group  $Fd3m$  unit cell displaying an occupation represented by  $(Zn_x^{2+}Fe_{1-x}^{3+})[Ni_x^{2+}Fe_{1+x}^{3+}]O_4^{2-}$  [10, 11]. In this formula the transition metal ions inside the parentheses occupy the tetrahedral site D, while the metal ions inside the brackets occupy the octahedral site E.

Considering the absence of  $Zn^{2+}$  cations in the ferrite, the amount of iron in both atomic sites would be equal and their contribution to the magnetic dipole moment would be canceled, and the formation of the material magnetic dipole moment would be responsibility for  $Ni^{2+}$  cations. Doping the ferrite with  $Zn^{2+}$  cations, there is a migration of  $Fe^{3+}$  cations from tetrahedral sites to octahedral sites, unbalancing initial equality of  $Fe^{3+}$  cations. Therefore there is an abrupt increase in magnitude of the magnetic dipole moment, because  $Fe^{3+}$  and  $Zn^{2+}$  cations are contributing to the dipole moment of the material. Thus, it is possible to produce a large number of intrinsically magnetic ferrite by appropriate substitution of metallic ions. Figure 1 presents a representation of a portion of nickel-zinc ferrite with  $Ni_{0.5}Zn_{0.5}Fe_2O_4$  stoichiometry and structure type inverse spinel, with octahedral sites  $FeO_6$  or  $NiO_6$  in blue and tetrahedral sites  $FeO_4$  or  $ZnO_4$  in red.

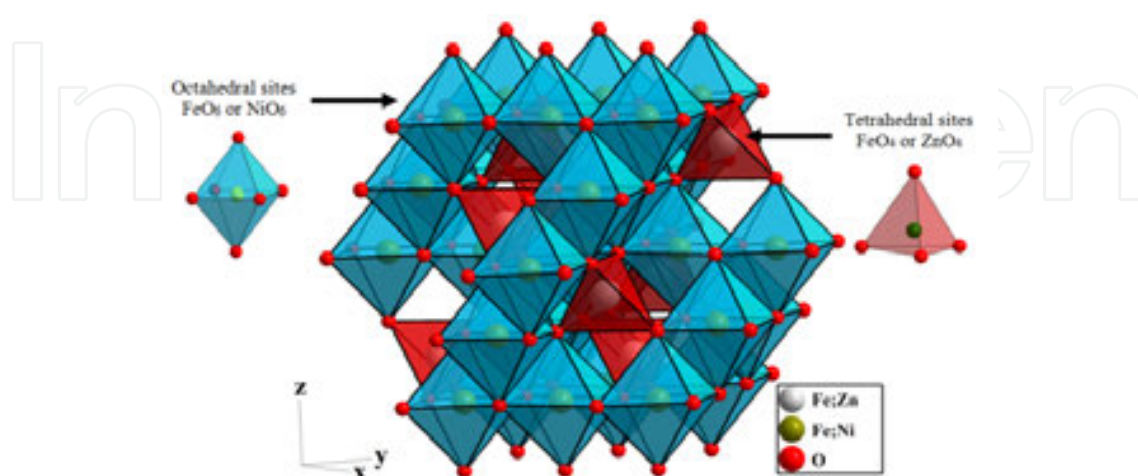


**Figure 1.** Oxide nickel-zinc ferrite representation, with stoichiometry  $Ni_{0.5}Zn_{0.5}Fe_2O_4$  with structure type inverse spinel. Octahedral sites  $FeO_6$  or  $NiO_6$  are presented in blue and tetrahedral sites  $FeO_4$  or  $ZnO_4$  are presented in red.

Regarding magnetic ceramics, Ni-Zn ferrites stand out and attract scientific community interest, due to its high electrical resistivity, differentiated magnetic properties and several technological applications in electronics, telecommunications and biotechnology [8]. They are generally used in cores of transformers and inductors for high-frequency microwave devices, telecommunication systems and radars, high-speed read and recording magnetic heads, cellular telephony, hospital equipments, among others. In microwave-absorption devices (e.g. electromagnetic interference shielding), absorption capacity may be generated/potentiated by altering material magnetic or dielectric properties [12].

### 1.3.2. TTB structure and potassium-strontium niobate

Tetragonal tungsten bronze (TTB) crystalline structure is considered a structure derived from classic perovskite, where the central octahedral structure  $\text{BO}_6$  is converted into three different types of cavities, tetrahedral and pentagonal tunnels similar to those found in perovskite structure which are favorable for substitution by cations, and trigonal tunnels are favorable for substitution by smaller cations and anions [9].

TTB structure can be described by chemical formula  $\text{A}'_2\text{B}'_4\text{C}'_4\text{Nb}_{10}\text{O}_{30}$ , where A', B' and C' represent different sites on the structure [13]. Depending on the number of sites available, TTB niobates are natural candidates to host structures, due to the possibility of a wide variety of cation substitutions, similar to what occurs with lead zirconate titanate ( $\text{PbZnTiO}_3$ ). B' cavity has a cube-octahedral coordination of oxygen atoms; A' cavities have pentagonal prismatic coordinations, while C' cavities have trigonal prismatic coordinations. The size of these cavities decreases following the order  $\text{A}' > \text{B}' > \text{C}'$ . In TTB-type compounds, alkali and alkaline earth metals are located at A' and B' sites, while only cations with small atomic radius such as Li are located in C' site. TTB-type compounds with formula  $\text{A}_6\text{Nb}_{10}\text{O}_{30}$ , A' = Sr or Ba exhibit semiconductor characteristics which can be incremented when dopants are added.

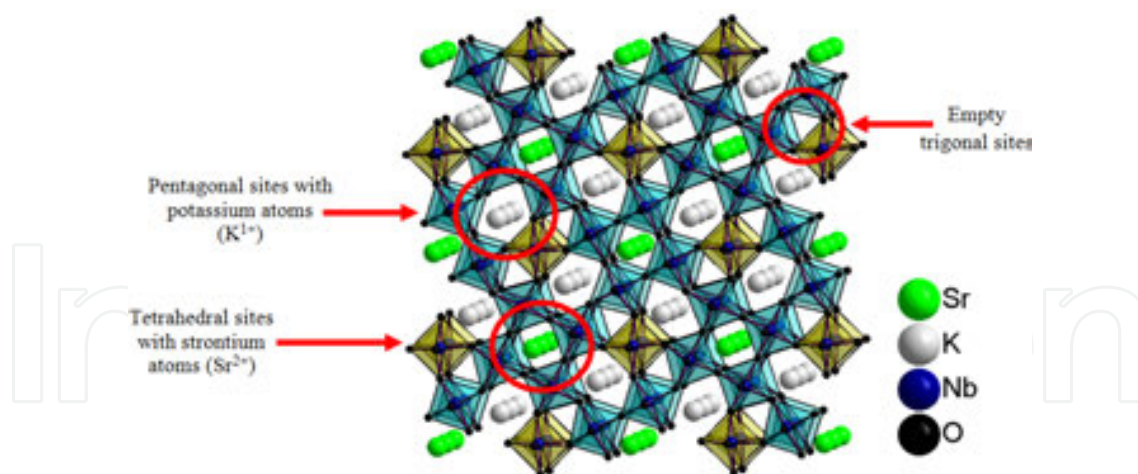
Niobates with TTB-type structure such as  $\text{KSr}_2\text{Nb}_5\text{O}_{15}$ ,  $\text{NaSr}_2\text{Nb}_5\text{O}_{15}$ ,  $\text{KBa}_2\text{Nb}_5\text{O}_{15}$ ,  $\text{NaBa}_2\text{Nb}_5\text{O}_{15}$  and  $\text{K}_3\text{Li}_2\text{Nb}_5\text{O}_{15}$  have created interest mainly by high anisotropy of the crystal structure. Among TTB-structure oxides, strontium potassium niobate oxide ( $\text{KSr}_2\text{Nb}_5\text{O}_{15}$ ) stands out for being a classic ferroelectric material with Curie temperature close to 430 K [14], belonging to a class of ceramic composites which have great potential application as sensing devices, actuators, memories, transducers, filters and capacitors.

Figure 2 shows a representation of strontium potassium niobate oxide structure, with oxygen and niobium octahedra in blue and yellow dark, pentagonal sites with potassium atoms ( $\text{K}^{1+}$ ), tetrahedral sites with strontium atoms ( $\text{Sr}^{2+}$ ) and vacant trigonal sites. This type of structure has two niobium types, which differ from each other by crystallographic position, multiplicity and occupancy factor. Nb(I) leads to  $\text{NbO}_6$  sites identified by their blue color, and Nb(II) leads to  $\text{NbO}_6$  sites identified by dark yellow color. The ratio between Nb atoms is 4 Nb(I) to 1 Nb (II).

## 1.4. Natural rubber

Latex is extracted from rubber tree stem, more specifically, from lactiferous vessels located in the cortex, and is responsible for bringing food to the tree top. From a chemical point of view,





**Figure 2.** Representation of strontium potassium niobate oxide (KSr<sub>2</sub>Nb<sub>5</sub>O<sub>15</sub>) with tetragonal tungsten bronze structure. Pentagonal sites occupied by atoms of potassium (K<sup>1+</sup>), tetrahedral sites occupied by atoms of strontium (Sr<sup>2+</sup>) and trigonal vacant sites are highlighted.

latex is a stable colloidal dispersion of a polymer in an aqueous medium. The dispersed polymer is aggregated in the form of particles with approximately spherical geometry (natural rubber micelles), with typical diameters between 30 and 1,000 nm [15].

The latex used in this work was collected from rubber trees of *Hevea brasiliensis* species, clone RRIM 600. This is a secondary clone developed by the Rubber Research Institute of Malaysia - RRIM, the most planted in the plateau region of São Paulo Brazilian state, due to its good performance and effect on production. This clone presents tall trees with vertical stem and fast growing when young. Its high production is highlighted, being one of the clones that has a higher dry rubber productivity.

Latex composition is, on average, 35% natural rubber (hydrocarbons), which compound is 2-methyl-1, 3-butadiene (C<sub>5</sub>H<sub>8</sub>), commercially known as isoprene. Recently-extracted latex is a neutral substance at room temperature with a pH between 6.0 and 7.2, depending on weather conditions, and density between 0.975 and 0.980 g/cm<sup>3</sup>. When exposed to air for 12 - 24 hours, latex pH decreases to values close to 5.0 and spontaneous coagulation process begins, separating rubber and non-rubber fractions. Rubber fraction can be represented by (C<sub>5</sub>H<sub>8</sub>)<sub>n</sub>, where n is the number of monomers in the chain (between 2,000 and 10,000), presenting an average molecular weight from 600,000 to 950,000 g/mol.

Figure 3 presents the *Hevea brasiliensis* cultivation (a), the bleeding process, in order to collect latex (b), and dry natural rubber, "Brazilian pale crepe" type (*Crepe Claro Brasileiro* - CCB) (c).

### 1.5. Nanocomposite materials

As commented by P. M. Ajayan and co-workers [16], the field of nanocomposites involves the study of multiphase material where at least one of the constituent phases has one dimension less than 100 nm. The promise of nanocomposites lies in their multifunctionality, the possibility of realizing unique combinations of properties unachievable with traditional materials. The



**Figure 3.** (a) Rubber tree plantation, *Hevea brasiliensis* species, (b) latex collection process using the bleeding method; detail: storage vessel, and (c) dry natural rubber, "Brazilian pale crepe" type.

challenges associate to this area are immense. They include control over the distribution in size and dispersion of the nanosize constituents, tailoring and understanding the role of interfaces between structurally or chemically dissimilar phases on bulk properties. Large scale and controlled processing of many nanomaterials has yet to be achieved.

An special class of composites and nanocomposites is the one formed by polymer and ceramic materials. In general, choosing a polymer as a matrix or continuous phase is interesting, since many of them have appreciable mechanical and thermal properties. Other properties are also regarded, e.g. hydrophobic/hydrophilic balance, chemical stability and bio-compatibility. The nanometric component is usually inorganic, and called dispersed phase. It can provide high mechanical and thermal stability and novel properties and functionalities that depend on component chemical nature, structure, size and crystallinity [17]. The dispersed phase provides or improves the redox properties, electronic, magnetic, density, refractive index, and others. In most cases, the main features of each of the components present in the nanocomposite is preserved or even improved and, in addition, one can obtain new properties resulting from the synergy of both components. Typical examples of polymer/ceramic nanocomposites of technological interest are formed by ceramic nanoparticles such as barium strontium titanate phase in a matrix with low dielectric loss [18] or nickel-zinc ferrite ( $\text{Ni}_{0.5}\text{Zn}_{0.5}\text{Fe}_2\text{O}_4$  or NZF), dispersed in a polymeric matrix such as vulcanized natural rubber (NR) [19].

When mechanical properties of composites and nanocomposites are investigated, it is seen that the main contribution comes from the polymeric matrix. However, an appropriate nanoparticle engineering and dispersion process can act amplifying, reducing or creating new features in mechanical properties of nanocomposites. Interface and interaction between nanoparticles/matrix exert a significant influence on the mechanical properties, mainly due to the reorganization of chemical bonds and physical attractions of electrostatic nature. Therefore, properties of nanoparticles such as shape, size, surface activity, crystallinity and network microstrain become relevant. Depending on nanocomposites composition, external factors such as temperature, application of electric and magnetic fields can alter and modulate their properties, expanding application options for these materials. Thus, nanocomposites can be used in intelligent membranes, new catalysts and sensors, new generations of photovoltaic and fuel cells, intelligent micro-electronics systems, micro-optical and photonic components,

and also therapeutic systems that combine marking, visualization, therapy and control of drug release [20, 21].

## 2. Employed methods

In the next topics, the preparation methods used in nanoparticles synthesis will be explored. The nanoparticles mentioned are magnetic (nickel-zinc ferrite, with stoichiometry  $\text{Ni}_{0.5}\text{Zn}_{0.5}\text{Fe}_2\text{O}_4$  (NZF)), ferroelectric (strontium potassium niobate, stoichiometry  $\text{KSr}_2\text{Nb}_5\text{O}_{15}$  (KSN)), besides magnetic and ferroelectric nanocomposites based on vulcanized natural rubber. Characterization techniques used are also covered, as well as biological testing of cell viability and against leishmaniasis.

### 2.1. Preparation of ceramic nanoparticles

Preparation of ceramic phases  $\text{KSr}_2\text{Nb}_5\text{O}_{15}$  (KSN) and  $\text{Ni}_{0.5}\text{Zn}_{0.5}\text{Fe}_2\text{O}_4$  (NZF) was performed using Modified Polyol Method [22, 23]. The main advantages of this method are high chemical homogeneity, the possibility of obtaining single phase powders and the large material portion produced in a single synthesis process (10 to 100g). Chemical formula and purity of starting reagents employed in oxides synthesis are listed in Table 1.

Component	Chemical formula	Purity
<b>Fuel for nanoparticles synthesis</b>		
Ethylene glycol	$\text{C}_2\text{H}_4(\text{OH})_2$	P.A.
Nitric acid	$\text{HNO}_3$	65%
<b><math>\text{KSr}_2\text{Nb}_5\text{O}_{15}</math> nanoparticles</b>		
Strontium carbonate	$\text{SrCO}_3$	P.A.
Potassium carbonate	$\text{K}_2\text{CO}_3$	P.A.
Niobium complex salt	$\text{NH}_4\text{H}_2[\text{NbO}(\text{C}_2\text{O}_4)_3] \cdot 3\text{H}_2\text{O}$	P.A.
<b><math>\text{Ni}_{0.5}\text{Zn}_{0.5}\text{Fe}_2\text{O}_4</math> nanoparticles</b>		
Nickel oxide	$\text{Ni}_2\text{O}_3$	P.A.
Zinc oxide	$\text{ZnO}$	P.A.
Iron oxide	$\text{Fe}_2\text{O}_3$	P.A.

**Table 1.** Chemical formula and purity of the materials used in the preparation of ferroelectric and paramagnetic nanoparticles (respectively,  $\text{KSr}_2\text{Nb}_5\text{O}_{15}$  and  $\text{Ni}_{0.5}\text{Zn}_{0.5}\text{Fe}_2\text{O}_4$ ).

- **Description:** in a 2 L beaker, under stirring and heating, the dissolution in nitric acid of all precursor oxides was performed in proper proportion to the desired oxide stoichiometry. 50 g of niobate oxide and ferrite were prepared for each synthesis and stoichiometric



calculations were based on this mass value. Upon dissolution of all starting materials, 100 ml of ethylene glycol were added. In a chapel, the temperature was raised to 180 °C using a magnetic stirrer. With the gradual increase of temperature occurred the emanation of a yellowish-brown coloured gas, due to decomposition of NO<sub>3</sub> groups, similar to the process developed in synthesis via Pechini method [24]. After this initial process, the material generated in the beaker was placed in a chamber-type oven.

- **Pre-calcining:** precursors pre-calcination was carried out in two stages, under an O<sub>2</sub> atmosphere with a flow of 500 ml/min for the niobate phase and under a N<sub>2</sub> atmosphere with a flow of 300 ml/min for the ferrite phase. In the first step, the temperature was increased from room temperature at a rate of 10 °C/min to 150 °C, which was held constant for 2 hours for elimination of low molecular mass molecules such as water vapor and some organic groups. In the following, keeping the same heating rate, temperature was raised to 300 °C and maintained for 1 h, in order to remove part of non-stoichiometric elements of the phase. During pre-calcination significant elimination of organic material fraction occurs, thus obtaining a black precursor powder for KSN and reddish-brown powder for NZF.
- **Calcination:** Both precursors were calcined with a final temperature of 450 °C. For niobate phase, a ten-hour threshold (600 m) was performed at 300 °C for disposal of organic wastes, and a two-hour threshold (120 m) in the final calcination temperature. A heating rate of 5 °C/min and nitrogen flow of 150 mL/min were used during heating, for avoiding sample oxidation in second phase formation. For ferrite, a three-hour threshold (180 minutes) was performed at final calcination temperature, in order to provide sufficient time for occurring of diffusional mass processes. A heating rate of 5 °C/min and air flow equal to 7 L/min were used during heating. For both phases, the cooling process was performed at a natural rate.

Figure 4 presents a flowchart of the steps for preparing and calcining the niobate and ferrite by modified Polyol method until to characterization stage.

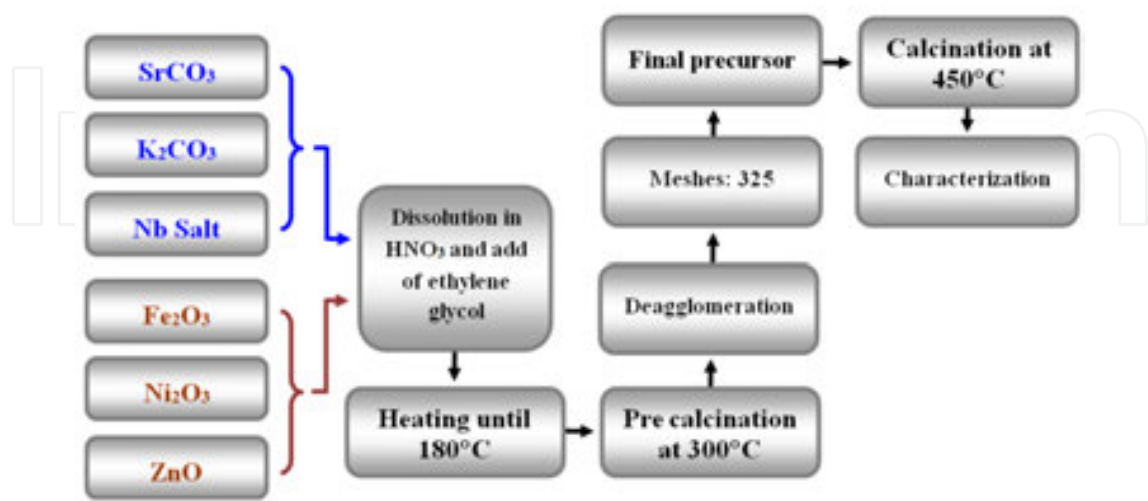


**Figure 4.** Flowchart of ferroelectric KSnNb<sub>5</sub>O<sub>15</sub> and paramagnetic Ni<sub>0.5</sub>Zn<sub>0.5</sub>Fe<sub>2</sub>O<sub>4</sub> ceramic phases preparation by Modified Polyol Method. In blue, starting reactants from phase KSnNb<sub>5</sub>O<sub>15</sub> and in red, starting reactants from phase Ni<sub>0.5</sub>Zn<sub>0.5</sub>Fe<sub>2</sub>O<sub>4</sub>.

## 2.2. Nanocomposite magnetic and ferroelectric preparation

Magnetic and ferroelectric nanocomposites were obtained from mechanical blending of dry natural rubber, various concentrations of ceramic nanoparticles and vulcanization system. Chemical formula and purity of the starting reactants employed in preparation of vulcanized natural rubber nanocomposites are listed in Table 2.

Component	Chemical formula	Purity
<b>Nanocomposites</b>		
Natural Rubber	$(C_5H_8)_n$	-
Zinc oxide	ZnO	P.A.
Stearic acid	$CH_3(CH_2)_{16}COOH$	P.A.
Mercaptobenzothiazole	$S_2NC_7H_5$	P.A.
Sulfur	$S_8$	P.A.

n: number of monomers in the polymer chain, between 2, 000 and 10, 000.

**Table 2.** Names, chemical formula, and purity of materials used in preparation of functional nanocomposites based on vulcanized natural rubber.

Nanocomposites preparation was initiated with dry mechanical mixing of the activation system in a open chamber mixer for 20 minutes. The activation system consists of 4 phr of zinc oxide and 3 phr of stearic acid with various concentrations of nanoparticles and 100 phr of dry natural rubber. At this stage the samples are called “activated samples”. These samples were stored at a temperature of 25 °C and without light exposure for 24 hours.

After the storage step, vulcanization (2 phr of sulfur) and acceleration (1 phr of 2-mercapto-benzothiazole) agents were added to the activated samples by using the same mixing route. At this stage the samples are termed “accelerated samples”. Accelerated samples were then thermo-conformed in thicknesses equal to 200 µm, 2 mm and 6 mm in a press with a heating system at 150 °C for 8 min and 30 s, and closing uniaxial pressure equal to 2.5 MPa. Vulcanization temperature and pressure used are indicated for natural rubber [25], and the vulcanization time parameter can be determined through rheometry test [26, 27].

Two sets of vulcanized natural rubber nanocomposites were prepared. The first set (NR/KSN) with  $KSr_2Nb_5O_{15}$  ferroelectric nanoparticles, and the second set (NR/NZF) with  $Ni_{0.5}Zn_{0.5}Fe_2O_4$  nanoparticles, both at various concentrations (1, 2, 3, 4, 5, 10, 20 and 50 phr). Figure 5 presents NR, NR/NZF and NR/KSN films and membranes with 5 phr of nanoparticles. Images of other samples with different concentrations and temperatures are visually similar and were not included in this section.

## 2.3. Main characterizations of nanoparticles and nanocomposites

- **XDR:** characterization by X-ray diffraction of KSN and NZF phases was performed on a X-ray diffractometer with Cu-K $\alpha$  radiation ( $\lambda = 1.54060 \text{ \AA}$ ), angular range of  $5^\circ \leq 2\theta \leq 80^\circ$ , and variation rate (or step) of  $0.02^\circ$ . Diffraction data were refined using the software FullProf

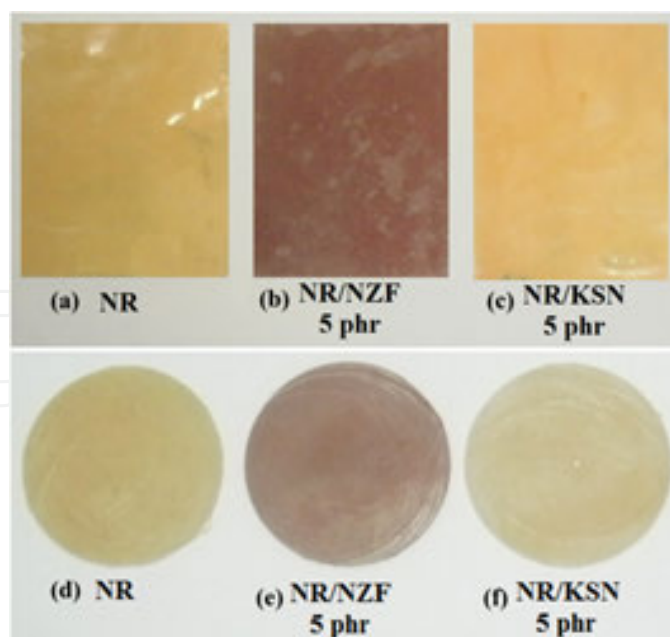


**Figure 5.** Thin films with a thickness of 200  $\mu\text{m}$  (a, b and c) and membranes with a thickness of 2 mm (d, e and f) of NR, NR/NZF, NR/KSN and NR/KSN/NZF respectively, with 5 phr of nanoparticles.

[28]. KSN, with a bronze tungsten tetragonal structure was indexed to JCPDS-34-0108 and NZF, with a inverse spinel structure was indexed to JCPDS-08-0234 [29].

- **TEM:** images of transmission electron microscopy of KSN and NZF nanoparticles at a temperature of 25  $^{\circ}\text{C}$  were obtained from the supernatant fraction of the dispersion, nanoparticles and methanol, deposited on a polymer film. A field-emission (FEG) microscope with tungsten filament was used; accelerating voltage between 40 and 100 kV, CCD chamber.
- **SEM:** scanning electron microscopy images of vulcanized natural rubber and nanocomposites NR/KSN and NR/NZF were performed using a microscope with field emission (FEG) and energy dispersive analysis of x-ray analysis (EDX). Images were obtained on the sample and cryogenically fractured surfaces.
- **AFM:** atomic force microscopy AFM/STM was used in contact mode. AFM were performed to characterize nanoparticles morphology, vulcanized natural rubber and functional nanocomposites. The public domain software Gwyddion was used to generate the three-dimensional projection of the sample surface from the height mode AFM images (height).

#### 2.4. Cell viability or toxicity assays

Assays of cell viability or the nanoparticles toxicity, vulcanized natural rubber and nanocomposites compared to mammalian cells were performed using “violet crystal method”, as described by J. Moraes et al [30]. Mammalian cell lineage used in these experiments was of Vero cells ATCC CCL-81, originating from “American Type Culture Collection” (Manassas, VA, USA), a cell line from African green monkey *Cercopithecus aethiops* (L.) kidney. In the

experiments, Vero cells were grown in culture plates of 96 wells containing nanoparticles at concentrations between 15.6 and 1000  $\mu\text{g/mL}$  or nanocomposites based on vulcanized natural rubber at concentrations between 250 and 4000  $\mu\text{g/mL}$  in DMEM (Dulbecco's Modified Eagle Medium) environment, supplemented with 10% serum at 37 °C in an  $\text{CO}_2$  atmosphere of 5%. Anova and Kruskal-Wallis tests were used to compare multiple normal or non-normal samples, respectively. Student's t-tests and Mann-Whitney test were used to compare two normal or non-normal samples, respectively. The BioEstat 5.0 software package [ACHO QUE ERA LEGAL COLOCAR UMA NOTA DE RODAPÉ FALANDO SOBRE ONDE OBTER O PROGRAMA] (Belém, Brazil, 2007) was used for performing the statistical tests and for graphical representations.

After 24 and 48 hours, supernatants were removed and adhered cells were fixed and stained with crystal violet 0.2% in methanol 20%v. It is noted that tests were carried out with concentrations of 150 mg/ml, concentrations significantly higher than those reported in the literature and no significant changes were observed as compared to essays up to 4000  $\mu\text{g/mL}$ . Toxicity was evaluated from the absorbance of control wells containing cells in DMEM environment. Throughout the incubation period, cultures were monitored daily in inverted optical microscope. All assays were performed in triplicate and the obtained average standard deviation was less than 2%.

#### 2.4. Leishmaniasis assays

*In vitro* population growth kinetics: In a BHI (brain heart infusion) environment supplemented with 10%v fetal bovine serum (FBS), 2% v human urine, 100  $\mu\text{g/mL}$  potassium G penicillin and 100  $\mu\text{g/mL}$  of streptomycin sulfate, a sample with rectangular dimensions 10x10x2mm of vulcanized natural rubber or nanocomposites with an inoculum of five hundred thousand parasites in the promastigote form of *Leishmania braziliensis* species, ARQ-1 strains isolated from clinical cases of Santa Cruz do Rio Pardo city, São Paulo state, in 1997.

From that instant, every three hours for a week, cell counts on the supernatant portion of the colony were performed using a Neubauer chamber. With data count a curve of parasite colony development was sketched. For comparison, control colonies, i.e. without the introduction of samples or natural rubber nanocomposites were also investigated. Throughout the tests, the temperature was maintained between 27 and 32 °C, and hydrogen potential (pH) between 6.0 and 6.9. All assays were performed in triplicate and the average standard deviation obtained was less than 1%.

### 3. Main results and discussions

To support discussions related to the applications of nanoparticles and magnetic and ferro-electric nanocomposites in cultures of Leishmaniasis, morphological and structural characterization of nanometric materials were performed. Thus, information is obtained mainly about the interaction of the nanoparticles and nanocomposites with the biological material, cooperating in the understanding of the results.

3.1. Structural and morphological nanoparticle essays

Figure 6 presents the diffraction pattern at room temperature for KSN and NZF nanoparticles, calcined at 450 °C for 2 hours. Lines and vertical bars represent experimental data and diffraction patterns respectively, categorized in JCPDS database: 34-0108 (KSN) and 08-0234 (NZF).

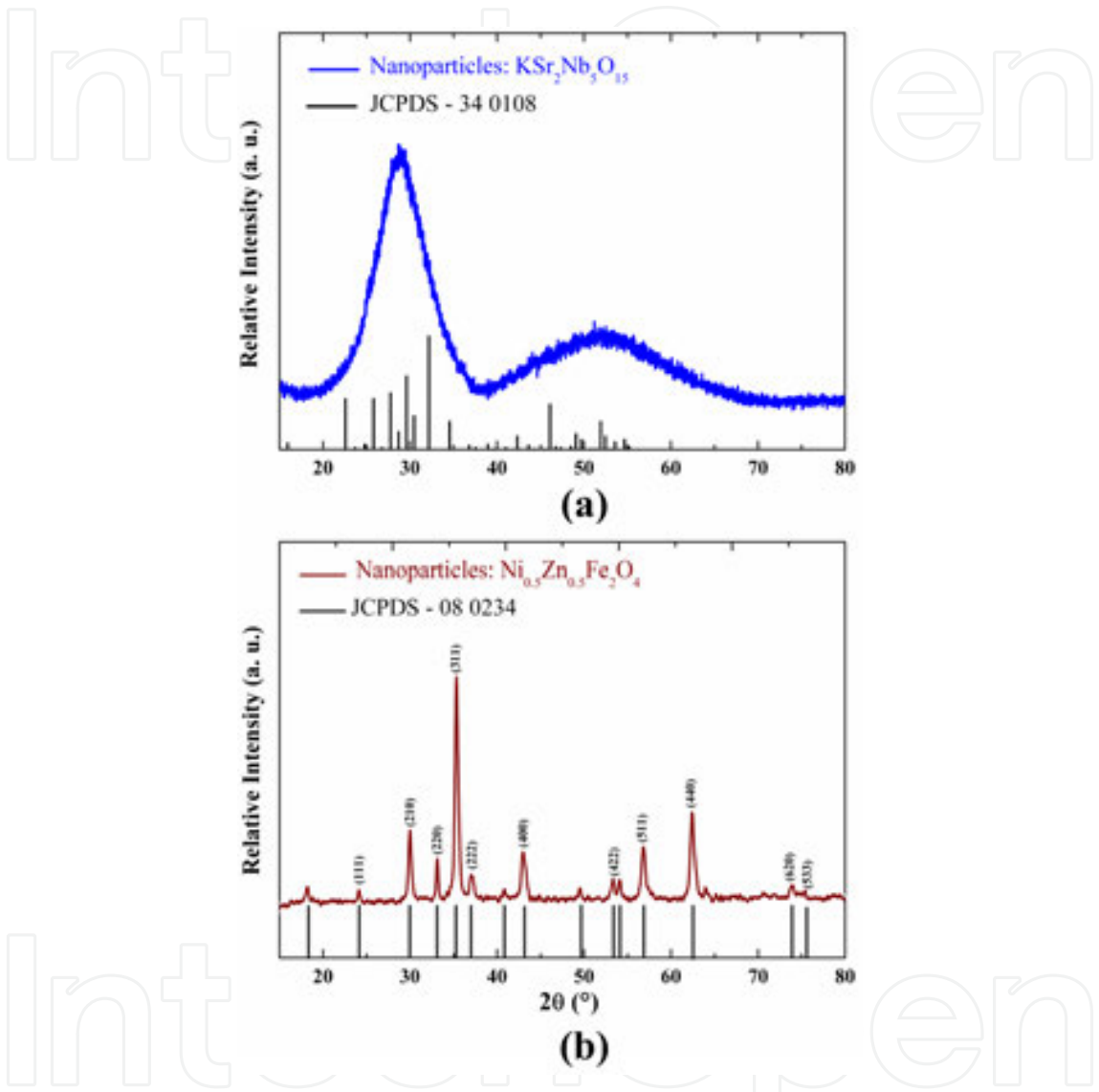


**Figure 6.** X-ray diffraction: (a) KSr<sub>2</sub>Nb<sub>5</sub>O<sub>15</sub> phase, calcined at 450 °C, together with experimental data, columns of the identity card JCPDS-34-0108 and (b) Ni<sub>0.5</sub>Zn<sub>0.5</sub>Fe<sub>2</sub>O<sub>4</sub> phase, calcined at the temperature of 450 °C, together with experimental data, columns of the identity card JCPDS-08-0234.

As can be seen in Figure 6, and according to studies conducted previously by the authors [31], the diffraction pattern obtained for the KSN shows the typical profile of a material with short-distance ordering (amorphous), identifying only two large sets of overlapping diffraction lines indicating that the thermal energy supplied during the heat treatment was not sufficient for obtaining a crystalline material. Relative crystallinity obtained for KSN was equal to approximately 10%, compared with the same material calcined at 1150 °C.



A diffractogram obtained for NZF phase displays a set of well-resolved diffraction lines, indicating that heat treatment was suitable for the production of a material with a high crystallinity degree, relative crystallinity of 74% when compared with the same material calcined at 650 °C. For KSN phase, the formation of a tetragonal tungsten bronze structure (TTB) with P4bm spatial group (No. 100) was identified, while for phase NZF the formation of a inverse spinel structure with space group Fd3m (No. 227) was identified. Network parameters "a", "b" and "c" obtained from KSN phase and "a" for NZF phase are equal to "a" = 12.4585 Å, "b" = "c" = 3.9423 Å and "a" = 8.394 Å, respectively. The unit cell volume is equal to  $V = 611.90 \text{ Å}^3$  and  $V = 591.435 \text{ Å}^3$  to KSN and NZF.

Average crystallite size, obtained by Scherrer's equation, was equal to 2 nm for KSN and 14.7 nm for NZF. Network microstrain ( $\gamma$ ), calculated by Williamson-Hall equation, was equal to 0.32 for KSN and 0.05 for NZF. Structural parameters obtained in this study are in agreement with values reported in previous publications [32, 33].

Figure 7 presents transmission electron microscopy (TEM) images at a temperature of 25 °C of KSN ferroelectric and NZF paramagnetic nanoparticles, both calcined at 450 °C, where (a) and (c) are 10, 000 times magnifications while (b) and (d) are 600, 000 times magnifications. The images (b) and (d) were generated from amplifications of specific regions of the images (a) and (c).

As can be seen in Figure 7 (b) and (d), for both types of primary particles, their geometry are approximately spherical due to nucleation-type particle growth mechanism, predominant in ceramic materials and also to the principle of surface energy minimizing. Average particle diameter of strontium potassium niobate is approximately 15 nm, while the average size for a primary particle of nickel-zinc ferrite is approximately 10 nm; both values are consistent with particle diameters in the scientific literature [32, 33] and agree with average-size crystallite values. As expected, KSN particle diameter for is larger than NZF particle diameter, due to the fact that tetragonal tungsten bronze structure (23 atoms/ minimal formula, pentagonal, tetragonal and trigonal sites) has greater complexity than cubic inverse spinel-type structure (7 atoms/minimal formula, octahedral and tetrahedral sites), thus the minimum cluster size to stabilize the particle tends to be higher for KSN than for NZF. Due to the difference of stage complexity, it is also expected that as both received the same heat treatment and then the same amount of thermal energy, NZF phase would be more crystalline than KSN phase, since NZF phase requires less energy to the atoms achieve their ideal atomic positions.

According to Figure 7 (a) and (c), one can identify that both ceramic phases present clusters even at nanometric scale, due to the action of secondary forces and coalescence phenomena. For KSN phase one can identify clusters with an average size of 80 nm or approximately 112 nanoparticles/cluster and for NZF phase, agglomerates with an average size of 100 nm or around 740 nanoparticles/cluster. For both estimates, clusters with spherical shape and a close-packing bundling type were considered [34]. In principle, magnetic properties displayed by NZF nanoparticles could contribute to formation of larger clusters when compared with non-magnetic phase clusters, as reported and discussed by E. M. A. Jamal et al., for nickel magnetic particles [35]. However, cluster formation is attributed essentially to preparation method used to synthesize ceramic nanoparticles; in this case, a chemical route.

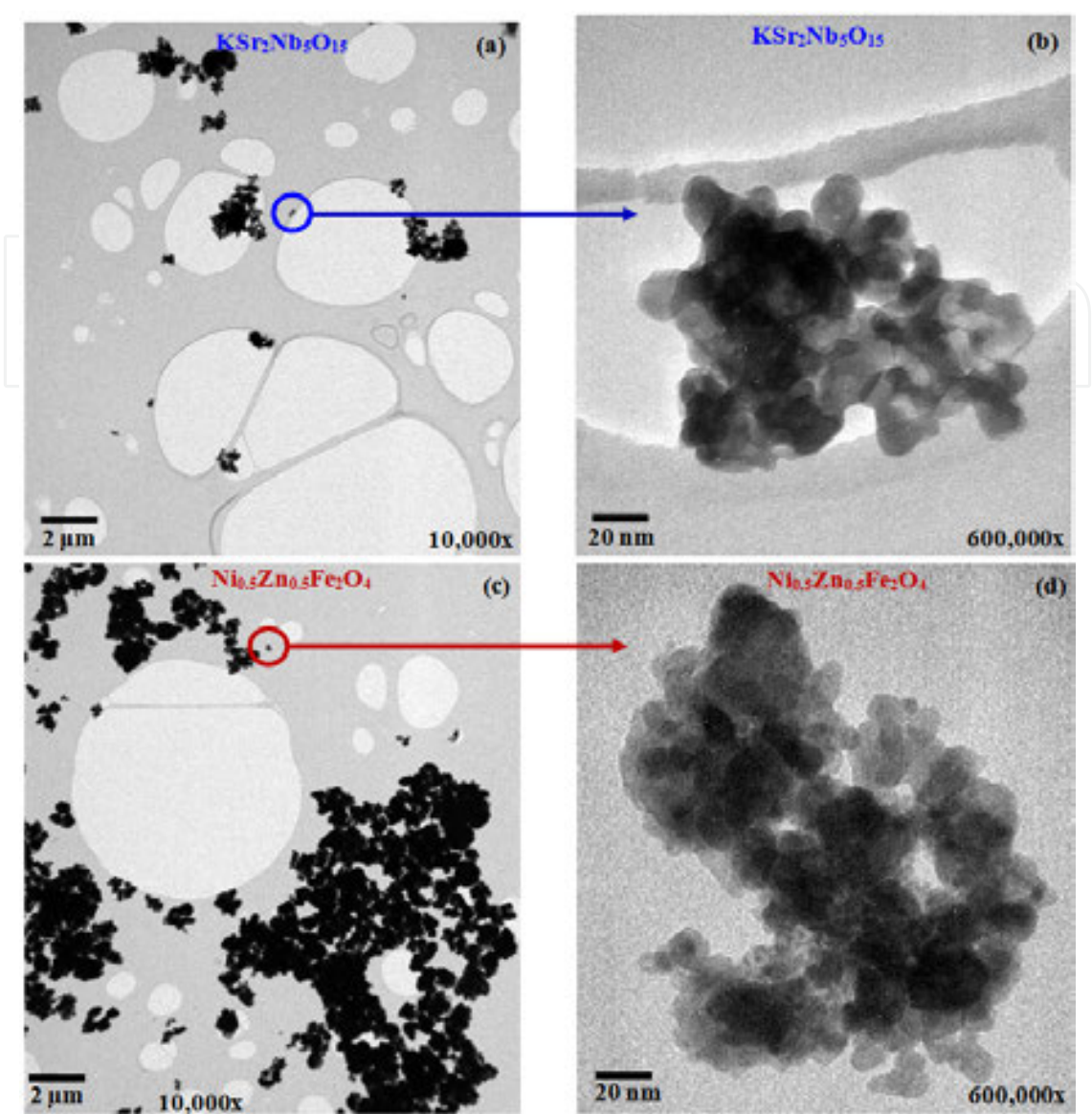


**Figure 7.** Transmission electron microscopy (TEM) at a temperature of 25 °C, of KSN ferroelectric [(a) and (b)] and NZF paramagnetic nanoparticles [(c) and (d)], calcined at 450 °C and at different magnifications.

Images acquired by Atomic Force Microscopy (AFM) at room temperature (25 °C) for KSN ferroelectric (a) and NZF paramagnetic nanoparticles (b) calcined at 450 °C are shown in Figure 8. Details on the grain boundary and the three-dimensional nanoparticle projection are given on the right.

According to Figure 8, structures on a nanometric scale were identified for both ceramic phases, in agreement with Figure 7. Images generated from amplitude data (main figure) provide qualitative information of nanostructure shape, while images generated from elevation data (three-dimensional projection) provide significant information about surface topography. Details on the grain boundary can be obtained from deflection data of the phase angle (image positioned in the third quadrant). For KSN ferroelectric nanoparticles, Figure 8 (a), a small

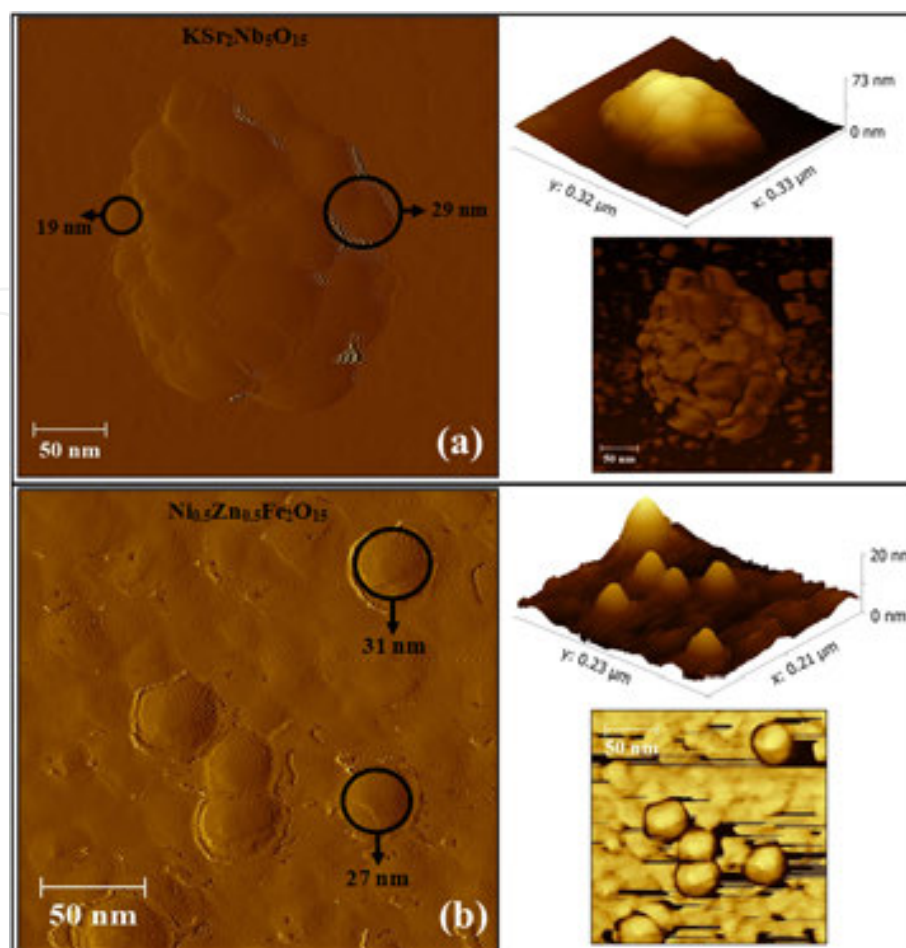


**Figure 8.** Atomic Force Microscopy (AFM) images generated from range, surface elevation and phase angle deflection data for KSN ferroelectric (a) and NZF paramagnetic nanoparticles (b). On the right, grain boundary details and three-dimensional nanoparticle projection.

cluster is observed in detail, with size approximately equal to 100 nm composed of nanoparticles with particle size distribution between 15 and 30 nm.

Small clusters formation is a typical feature of nanoscale materials processing using chemical routes. However, it is emphasized that the nanoparticles that compose the clusters are weakly linked together through secondary interactions of electrostatic origin. For NZF paramagnetic nanoparticles, Figure 8 (b), individual nanoparticles with approximately spherical geometry are identified, as well as the union of two or more nanoparticles by coalescence process. It is feasible to notice a particle size distribution between 25 and 40 nm for NZF phase. It should be noted that the particle size distribution for KSN and NZF is consistent with previously published work [36, 37].

### 3.2. Nanocomposite morphological study

Figure 9 presents scanning electron microscopy images obtained from the sample surface, a representation of the polymer chain and the EDX spectrum for the vulcanized natural rubber

NR/KSN-1phr ferroelectric and NR/NZF-1phr magnetic nanocomposites. Magnifications used were equal to 50, 000, 50, 000, and 150, 000 times.

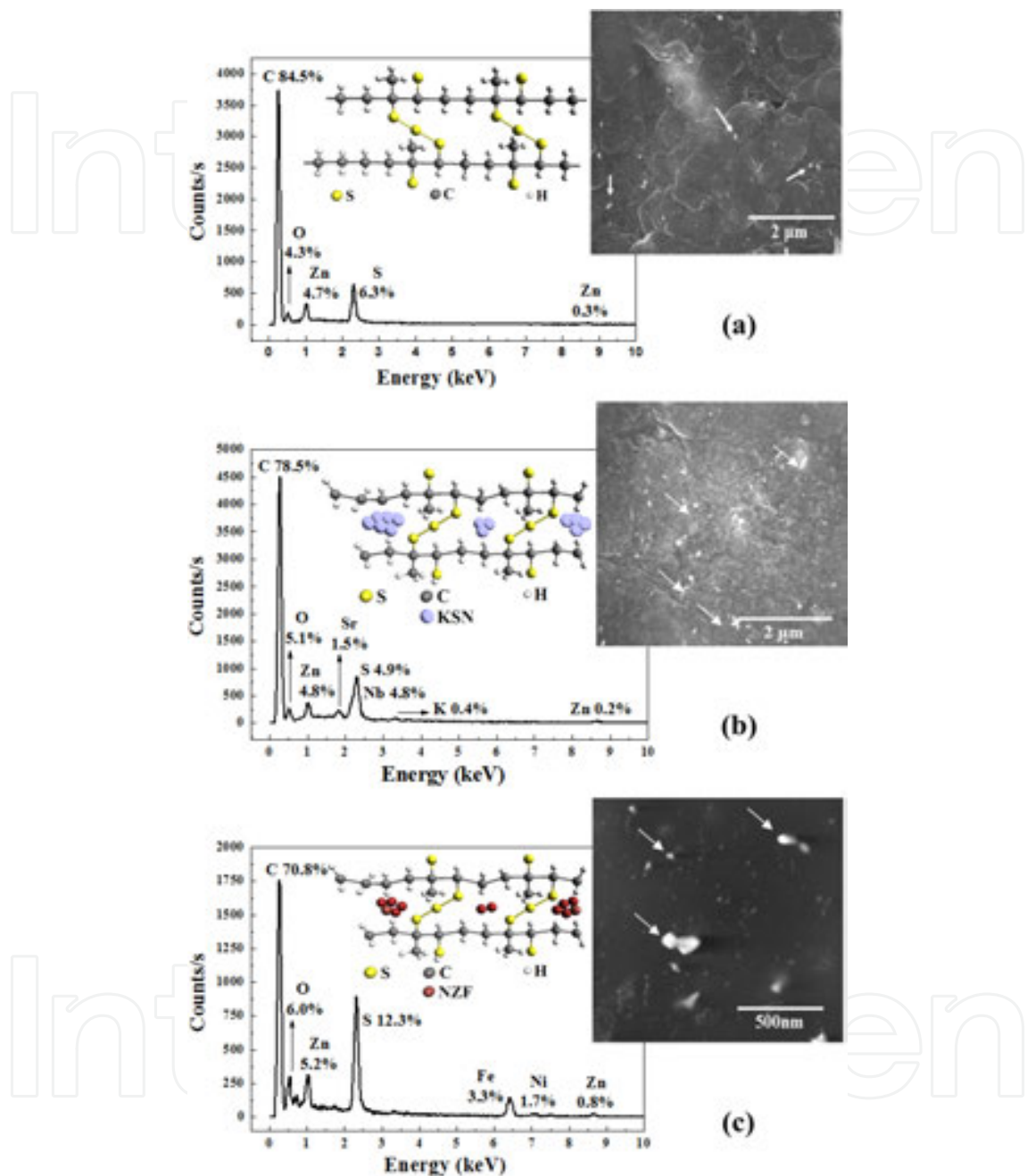


**Figure 9.** (a) Scanning electron microscopy images of the sample surface, polymer chain representation and EDX spectrum for vulcanized natural rubber, (b) ferroelectric nanocomposite NR/KSN-1phr and (c) magnetic nanocomposite NR/NZF-1phr.

In Figure 9 (a), a satisfactory surface homogeneity was observed, indicating that a vulcanization system in appropriate amounts and a efficient nanocomposite-preparing system was used. White spots were noticed and indicated with white arrows. Such points may be associated



with the vulcanization system, in agreement with the results obtained by XRD, particularly zinc and sulfur with submicrometer dimensions ( $> 250$  nm). According to Figure 9 (b) and (c), it is possible to identify a high dispersion of particles and small agglomerates with dimensions on the nanometer scale, between 20 nm and 80 nm, and a particle size in the submicron range.

It is suggested that the particles and small clusters are KSN and NZF nanoparticles, in accordance with the dimensional scale, dark grayish and reddish brown color in surface and inside of the nanocomposites, respectively. In EDX spectra, peaks of C, O, S and Zn were identified and are associated with the curing system and the polymer chains. EDX percentage differences observed for S and Zn among NR, NR/KSN-1phr and NR/NZF-1phr samples refer only to the position of the investigated sample and sample time exposure to X-ray.

Low percentages of K, Sr and Nb and Fe, Ni and Zn were found for samples of NR/KSN and NR/NZF and were assigned respectively to KSN and NZF nanoparticles. The values obtained are in agreement with the amount estimated by stoichiometric calculations. The difference in surface roughness observed in Figure 9 (a) and Figures 9 (b) and (c) may be associated to the mobility difference of the natural rubber polymer chain, due to the incorporation of nanoparticles, even in small mass quantities.

Images obtained by atomic force microscopy (AFM) for vulcanized natural rubber, NR/KSN-10phr ferroelectric nanocomposite and NR/NZF-10phr magnetic nanocomposite were performed directly on the surface of the samples, and their three-dimensional projections are presented in Figure 10, while Table 3 lists the values for NR surface roughness, NR/KSN ferroelectric and NR/NZF magnetic nanocomposites, depending on the nanoparticle concentration.

Sample	Superficial rugosity (nm)						
	NR	1 phr	3 phr	5 phr	10 phr	20 phr	50 phr
NR/KSN	0.45	0.68	0.83	0.70	0.55	0.50	0.58
NR/NZF	0.45	0.50	0.63	0.55	0.45	0.43	0.45

**Table 3.** Surface roughness values obtained from elevation mode AFM images, for vulcanized natural rubber (NR) and nanocomposites NR/KSN and NR/NZF.

According to Figure 10 and the data in Table 3, a satisfactory superficial homogeneity is noted for vulcanized natural rubber and both functional nanocomposites samples, suggesting that appropriate parameters and vulcanization system were used. Significant differences between the natural rubber nanocomposites were observed for surface roughness. At low nanoparticle concentrations, smaller than 3 phr, there is considerable roughness growth, followed by a reduction and stabilization of this parameter with increasing concentration of nanoparticles. This suggests that for low concentrations, local phenomena of elastomeric chain orientation as stress-induced crystallization [38, 39] can be significant.



Probably, differences in roughness identified between ferroelectric and magnetic nanocomposites are due to: (i) difference in interface between the nanoparticles that generate changes in polymer chains folding, (ii) different coefficients of thermal diffusion due to different ceramic phases and (iii) different anisotropies for polymer chains mobility [39].

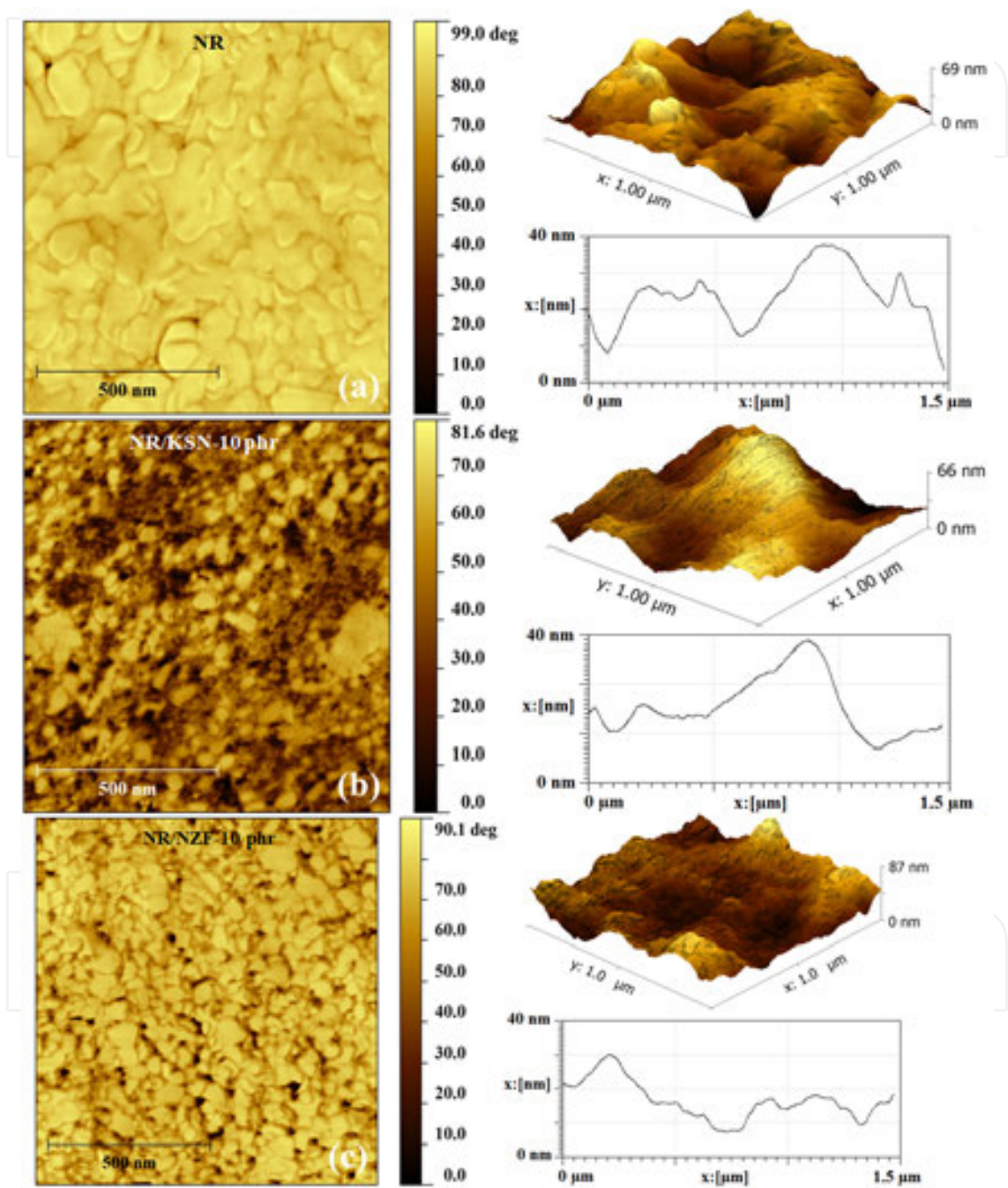


**Figure 10.** Images obtained using atomic force microscopy (AFM) to: (a) vulcanized natural rubber, (b) NR/KSN-10phr ferroelectric nanocomposite and (c) NR/NZF-10phr magnetic nanocomposite, performed directly on the surface of samples and their three-dimensional projections.

### 3.3. Polymer/ceramic composites and nanocomposites as an agent of control in Leishmaniasis colonies

Neglected diseases are illnesses that prevail not only in poverty conditions, but also contribute to the framework maintenance of economic and social inequality in the country (e.g. leishmaniasis, dengue, Chagas disease, schistosomiasis, leprosy and others [40]). As a result of this framework, multidisciplinary research involving materials science and biotechnology areas has gained significant strength, in order to develop new materials and methods to combat these diseases. For stimulating angiogenic processes [41] and due to its significant ability to disperse particulate fillers, natural rubber and its nanocomposites emerge as potential candidates for a new generation of bioactive agents with biocide character in biotechnology.

#### 3.3.1. Biological study: toxicity evaluation

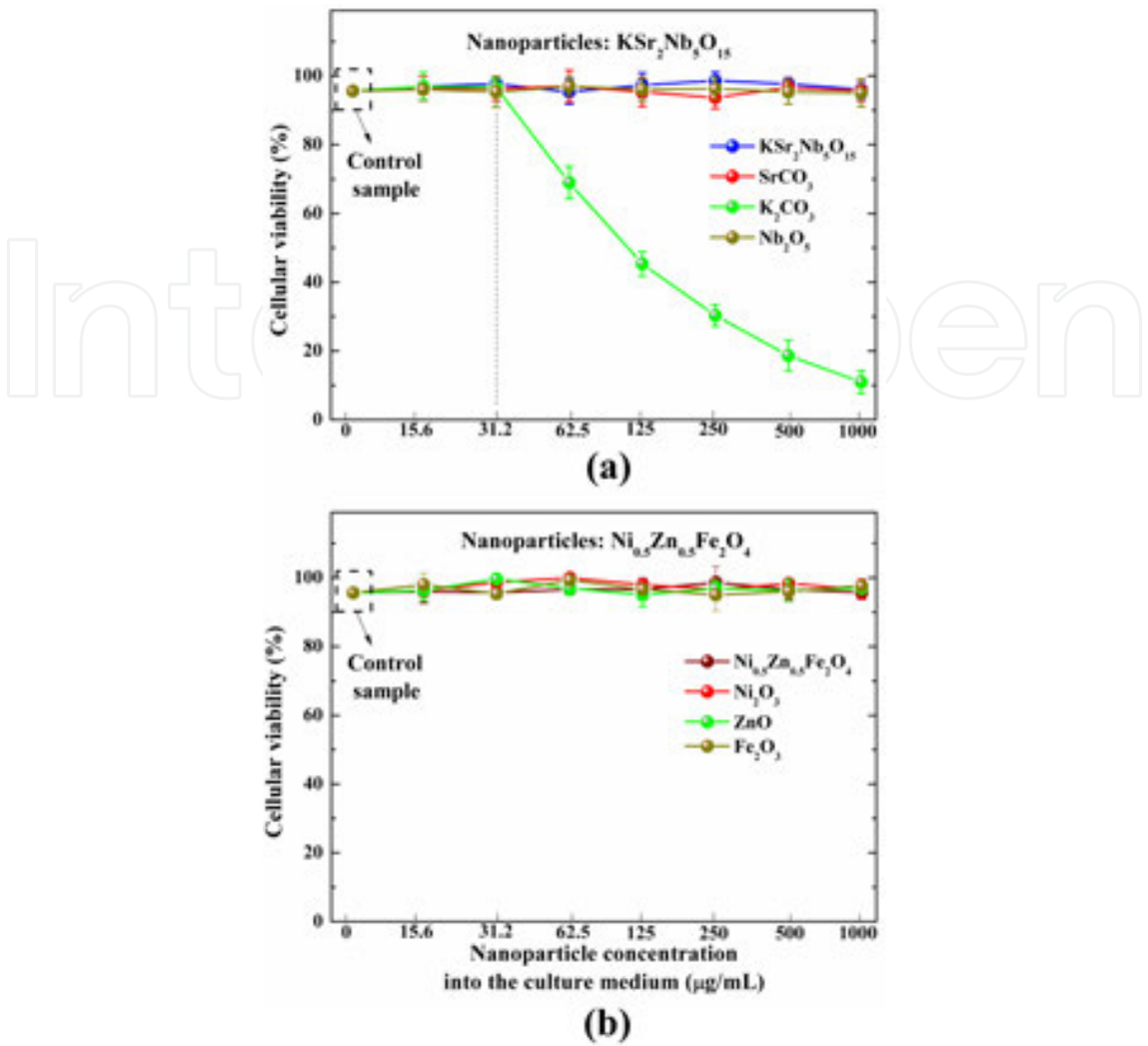
Due to great demand for innovation in biotechnology, nanoparticles and nanocomposites emerge as potential candidates for a new generation of biocides, and tests that assess the toxicity of these materials compared to mammalian cells comprises an important phase of the development process biotechnology.

Figure 11 presents the results of toxicity or viability evaluation of Vero cells after 48 h incubation in the presence of ceramic nanoparticles  $\text{KSr}_2\text{Nb}_5\text{O}_{15}$  and  $\text{Ni}_{0.5}\text{Zn}_{0.5}\text{Fe}_2\text{O}_4$  and their respective constituent elements, depending on particle concentration in the cellular environment [42].

According to Figure 11 for both ceramic phases and its constituent elements, except for potassium carbonate ( $\text{K}_2\text{CO}_3$ ), there is no statistically significant decrease in cell viability at the end of the incubation period until the maximal concentration tested in this case (1000  $\mu\text{g/mL}$ ), compared to cells incubated only in the culture environment.

For cells culture in contact with potassium carbonate particles, there is clearly a statistically significant reduction ( $P < 0.01$ ) in cell viability for concentration equal to or greater than 62.5  $\mu\text{g/mL}$ . Potassium carbonate in aqueous environment tends to dissociate, originating potassium ions ( $\text{K}^+$ ) that transform the extracellular environment, which should be hypotonic, in a highly hypertonic environment. Thus, cells pass for a excessive water-loss process through the cytoplasmic membrane and unbalances in key mechanisms for cell life maintenance, such as the sodium-potassium pump, mechanisms of nerve impulse conduction, protein synthesis and cell respiration. The combination of these processes is probably the responsible for the cell death observed for mammalian cells exposed to potassium carbonate particles. However, in  $\text{KSr}_2\text{Nb}_5\text{O}_{15}$  ferroelectric phase, potassium ions ( $\text{K}^+$ ) are isolated in the interstices of the crystallographic pentagonal structure (see Figure 4), which prevents the presence of these ions in the extracellular environment.

The results of toxicity or viability evaluation of Vero cells after 48 h incubation in the presence of vulcanized natural rubber NR/KSN ferroelectric and NR/NZF magnetic nanocomposites as a function of sample concentration in the cellular environment are shown in Figure 12. In detail, images generated by optical microscopy of cells exposed to NR/KSN-50 phr and NR/NZF-50 phr nanocomposites, and also the control sample.



**Figure 11.** Cell viability in the presence of (a) ferroelectric nanoparticles, (b) magnetic nanoparticles and their respective constituents on the basis of the concentration of particles present in the culture environment. Vero-type mammalian cells cultured in particles presence were used.

As can be seen in Figure 12, for vulcanized natural rubber and both classes of nanocomposites, regardless of nanoparticles concentration, it is not possible to observe a statistically significant reduction in cell viability at the end of the incubation period until the maximal concentration tested (in this case 4000  $\mu\text{g/mL}$ ), compared to cells incubated only in the culture environment. In both images generated by optical microscopy, cells attached to the substrate are observed, indicating that cells remain biologically viable and comparing the cells exposed image to the two nanocomposites types with cells grown freely, it is not possible to identify significant morphological alterations, confirming that mammalian cells were not significantly affected due to nanocomposites presence. So as significant reductions were not identified in cell viability when mammalian cells were exposed to  $\text{KSr}_2\text{Nb}_5\text{O}_{15}$  and  $\text{Ni}_{0.5}\text{Zn}_{0.5}\text{Fe}_2\text{O}_4$  nanoparticles, vulcanized natural rubber and nanocomposites, one can consider that such systems have potential for using in biological systems composed by mammalian cells.

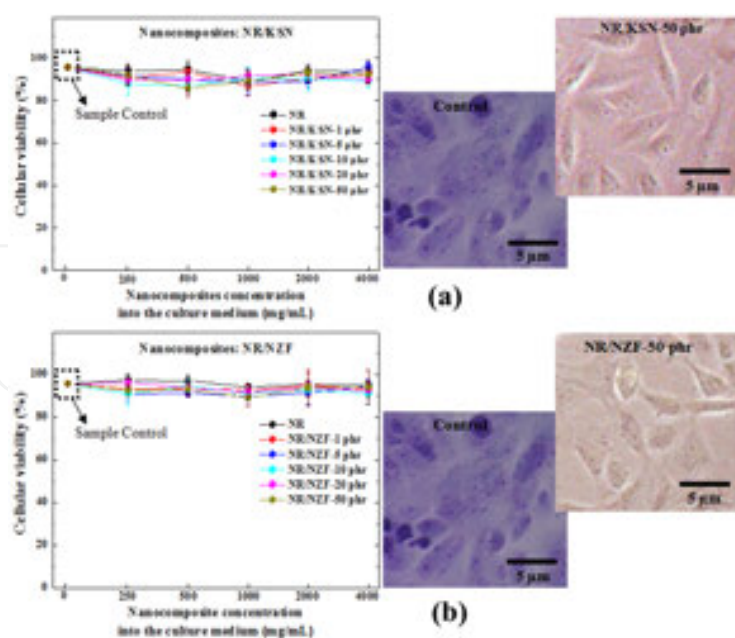


**Figure 12.** Cell viability in the presence of vulcanized natural rubber (a) NR/KSN ferroelectric and (b) NR/NZF magnetic nanocomposites as a function of sample concentration in the cell environment. In detail, images generated by optical microscopy of cells exposed and not exposed to nanocomposites. Vero-type mammalian cells were used, cultured in the presence of nanocomposites.

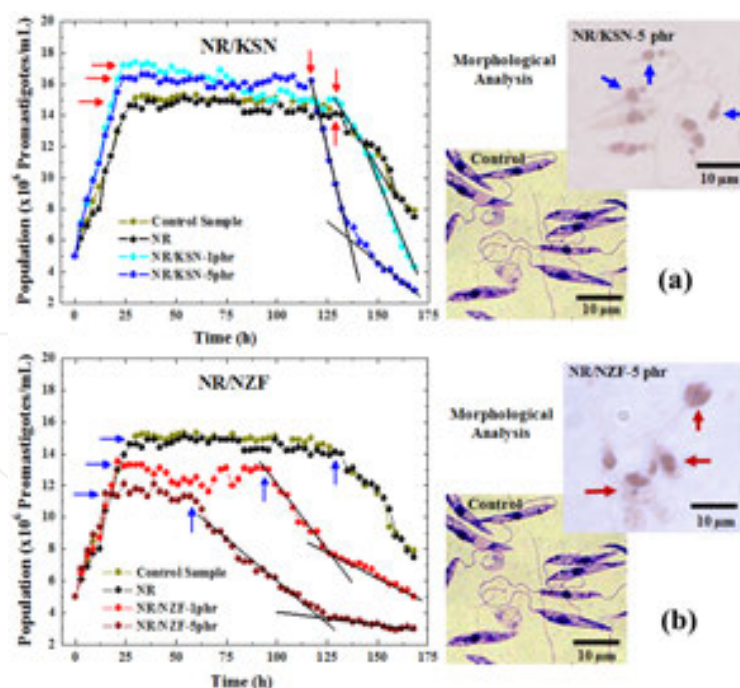


**Figure 13.** Population growth kinetics of *Leishmania braziliensis* (LB) parasite colony exposed to samples of vulcanized natural rubber, (a) NR/KSN and (b) NR/NZF nanocomposites. In detail, morphological comparison of parasites via optical microscopy.



Figure 13 presents the kinetics of colony population development of Leishmaniasis parasites exposed to vulcanized natural rubber samples, (a) NR/KSN ferroelectric and (b) NR/NZF magnetic nanocomposites in different nanoparticles concentrations. In detail, morphological comparison of the parasites after samples exposure.

Values for parameters maximum population density, phase duration, increase and decrease rates and also colony population of *Leishmania braziliensis* (LB) promastigotes exposed to samples of vulcanized natural rubber and nanocomposites are listed in Table 4.

Parameter	Sample								
	NR control	NR/KSN 1 phr	Δ%	NR/KSN 5 phr	Δ%	NR/NZF 1 phr	Δ%	NR/NZF 5 phr	Δ%
Generation time* (h)	14.4	9.3	-35%	9.7	-33%	13.1	-9%	12.0	-17%
Maximum population density (10 <sup>6</sup> parasites/mL)	15.1	17.2	+14%	16.4	+9%	13.5	-11%	11.5	-24%
Length of logarithmic phase (h)	30	24	-20%	24	-20%	21	-30%	15	-50%
Average growth of logarithmic phase (10 <sup>6</sup> cells/h mL)	0.3	0.51	+50%	0.48	+41%	0.4	+33%	0.4	+33%
Continuous phase duration (h)	102	108	+6%	93	-9%	75	-27%	42	-59%
Fall phase duration (h)	36	36	0%	51	+42%	72	+100%	111	+208%
Average rate of fall phase decrease (10 <sup>6</sup> cells/h mL)	0.2	0.3	+50%	0.3	+50%	0.1	-50%	0.05	-75%

\* Generation or double time: required time for doubling the cell population.

**Table 4.** Values for population development parameters of *Leishmania braziliensis* (LB) promastigotes colonies exposed to samples of natural rubber and vulcanized nanocomposites with different nanoparticle concentrations.

According to Figure 13 and data listed in Table 4, the increase curve evolution of LB promastigote population is similar for all samples studied, indicating that the presence of the samples did not change the colony global behavior. As expected, this evolution follows the standards of a colony of microorganisms grown in an artificial environment, being composed of three well-defined stages:



- **First stage:** denominated logarithmic phase, in which the pathogen has a large nutrient amount, conditions for their physiological maturation and mitotic cell division, a linear increase of promastigotes as a function of time is identified, and the average growth rate in this stage is higher for colonies exposed to samples. This suggests that the samples presence in the culture environment promotes the cell nutrition process;
- **Second stage:** denominated continuous phase, in which stabilize the processes of cell division, the parasites are mature and new members of the population do not arise; a constant number of promastigotes in function of time was identified. Oscillations in population density observed in this phase are due to cell death and reproduction, dependent on the environment nutritional availability or possible interaction between the parasite and the nanocomposite;
- **Third stage:** denominated fall phase, in which the nutritional resources of the culture environment are reduced and the process of cell death by depletion of internal micro-organism begins. A decreasing linear is identified, depending on time for control colony, and for the colonies exposed to vulcanized natural rubber samples and also linear decreasing for colonies exposed to samples of both nanocomposites and both nanoparticle concentrations, but with two different decrease rates, suggesting that there could be generations of parasites more resistant to the presence of samples in the colony, because they have already been evolved in nanocomposites presence.

Comparing the results for the control colony and the colony with a sample of vulcanized natural rubber samples, there is no statistically significant alterations in the of population growth kinetics, thus keeping unchanged the stages of cell development and maturation. However, for colonies exposed to nanocomposite samples having both nanoparticles, there are significant changes in microbial growth patterns. It should be mentioned that, regardless of the nanoparticle type associated with natural rubber, when the concentration of nanoparticles increases, the differences between the growth curves accentuate.

There is a progressive increase in the population of promastigotes in the logarithmic phase of the colonies exposed to NR/KSN nanocomposites (Figure 13 (a)), indicating that or KSN nanoparticles could come loose from nanocomposite surface, or something related to the interaction between the nanoparticles and the polymeric matrix is generating a change of or electronic nature significant structural proteins in the medium such that the parasites are able to ingest larger amounts of nutrients coming then to be reproduced more frequently. This hypothesis corroborates the reduction of over 30% in the generation time of the colonies.

The largest amount of immature parasites generated in logarithmic phase justifies the reduction in hours of the stationary phase, since the presence of large parasite quantities implies in a reduction of the amount of nutrients per parasite. It is worth mentioning that the population decrease noted in fall phase is intensified with increasing nanoparticles concentration in the nanocomposite, indicating that probably the same reason that is causing changes in culture proteins, facilitating their ingestion, is also hindering the absorption of these proteins by the parasites, accelerating nutritional starvation. Comparing the morphological characteristics of the parasites exposed to NR/KSN-5phr nanocomposites with colony control parasites [43, 44],

one could clearly identify the kinetoplast and nucleus cell, but no significant morphological differences were observed, confirming the similarity of the curves in Figure 13 (a).

In the case of the colonies exposed to NR/NZF nanocomposite samples (Figure 13 (b)), one can identify a linear decrease in intensity of the logarithmic phase, depending of increasing concentration of nanoparticles, indicating that the presence of such nanoparticles difficult culture protein consumption and cell division by the parasite. However, a slight reduction (lower than 20%) can still be noticeable to the generation time of the colonies. With a smaller amount of parasites in culture and limited capacity of nutritional consumption in the environment, there is a smaller stationary phase and a fall phase greater than that of control colonies than the sample and exposed to natural rubber samples.

Comparing the morphological characteristics of the parasites exposed to NR/NZF-5phr nanocomposites with colony control parasites [43, 44], there is a clear morphological difference in cell design. Control parasites has elongated cell bodies, while for parasites in contact with NR/NZF-5phr, the cell body has approximately a circular shape.

Whereas both types of nanoparticles have nanometric sizes, the first factor to justify the identified differences is that the sum of factors such as differences in crystallinity, surface area, micro-deformations of the crystal lattice, cell volume and especially chemical composition that generate surface characteristics particular to each nanoparticle type is responsible for the differences noted in each colony. However, intrinsic interactions between cells and magnetic/ferroelectric nanoparticle properties, which would help to explain the high specificity exhibited by nanoparticles against leishmaniasis parasites and not against mammalian cells can not be discarded, although less likely.

## 4. Conclusions

Modified polyol method was used in the chemical synthesis of potassium strontium niobate ferroelectric oxide with stoichiometry  $\text{KSr}_2\text{Nb}_5\text{O}_{15}$  and of nickel zinc ferrite paramagnetic oxide, stoichiometry  $\text{Ni}_{0.5}\text{Zn}_{0.5}\text{Fe}_2\text{O}_4$ . Single-phase ceramic phases with average crystallite size in nanometric scale were obtained. Using XRD and AFM essays, average crystallite size and particle surface parameters could be determined, mainly. We employed a method for the preparation of functional composites and nanocomposites based on vulcanized natural rubber, grounded in the dry mixing of the constituents using a open chamber mixing. A vulcanization system based on sulfur ( $\text{S}_8$ ), suitable for natural rubber and ceramic nanoparticles was used. The development of a potential application for composites and nanocomposites based on vulcanized natural rubber was started and the preliminary results are encouraging, namely: use of paramagnetic and ferroelectric nanocomposites as modulating agents of the development of colonies of *Leishmania braziliensis* parasites.

## Acknowledgements

The authors would want to acknowledge the Brazilian research agencies FAPESP, CAPES and CNPq for financial support, the graduate program of Materials Science and Technology, Carlos Gomes Barbosa-Filho and Dr. Josué de Moraes for the biological tests, Dr. José Antonio de Saja-Saéz, Prof. Dr. Miguel-Ángel Rodríguez-Pérez and Dr. Marcos Augusto de Lima Nobre for the scientific discussions and also Dr. Ricardo F. Aroca and Ariel Guerrero for the AFM measurements.

## Author details

Aldo Eloizo Job\*, Alexandre Fioravante de Siqueira, Caroline Silva Danna, Felipe Silva Bellucci, Flávio Camargo Cabrera and Leandra Ernst Kerche Silva

\*Address all correspondence to: [job@fct.unesp.br](mailto:job@fct.unesp.br)

Department of Physics, Chemistry and Biology, Univ Estadual Paulista, Presidente Prudente, Sao Paulo, Brazil

## References

- [1] Schneider P, Schmidt G. Nanocomposite polymer hydrogels. *Colloid Polym Sci.* 2009;287: 1-11.
- [2] Bellucci FS et al. Preparation and structural characterization of vulcanized natural rubber nanocomposites containing nickel-zinc ferrite nanopowders. *J. Nanosci. Nanotechnol.* 2012; 12(3): 2691-2699.
- [3] Oriakhi CO. Polymer nanocomposition approach to advanced materials. *J. Chem. Educ.* 2000; 77(9): 1138-1146.
- [4] Moraes J et al. *Schistosoma mansoni*: In vitro schistosomicidal activity of pipartine. *Exp. Parasitol.* 2011; 127: 357-364.
- [5] Joseph OH, Robert JN, Frank MC. Advantages of measuring changes in the number of viable parasites in murine models of experimental Cutaneous Leishmaniasis. *Infect. Immun.* 1983; 39(3): 1087-1094.
- [6] Sepulveda C., editor. *Leishmaniasis: Symptoms, Treatment and Potential Complications.* Nova Publishers; 2013.
- [7] Lindoso JAL et al. Review of the current treatments for leishmaniasis. *Research and Reports in Tropical Medicine.* 2012;3: 69-77.

- [8] Li XS et al. Synthesis and applications of functionalized magnetic materials in sample preparation. *Trends Anal. Chem.* 2013;45: 233-247.
- [9] Lanfredi S et al. Síntese e Caracterização Estrutural do Niobato de Potássio e Estrôncio com Estrutura tipo Tetragonal Tungstênio Bronze (TTB). *Cerâmica.* 2005;51: 151-156.
- [10] Zahi S. Synthesis, permeability and microstructure of the optimal nickel-zinc ferrites by sol-gel route. *J. Electromagn. Anal. App.* 2010;2: 56.
- [11] Sharma S et al. Influence of Zn substitution on structural, microstructural and dielectric properties of nanocrystalline nickel ferrites. *Mater. Sci. Eng., B.* 2010;167: 189.
- [12] Pessoa F. Síntese e caracterização de ferrita de níquel e zinco nanocristalina por combustão, para aplicação em compósito elastomérico absorvedores de micro-ondas. MSc dissertation. UFRJ; 2006.
- [13] Lanfredi S. Structural characterization and Curie temperature determination of a sodium strontium niobate ferroelectric nanostructured powder. *J. Solid State Chem.* 2011;184(5): 990-1000.
- [14] Das PS et al. Electrical properties of  $\text{Li}_2\text{BiV}_5\text{O}_{15}$  ceramics. *Physica B.* 2007; 395: 98-103.
- [15] Wititsuwannakul R et al. A rubber particle protein specific for Hevea latex lectin binding involved in latex coagulation. *Phytochemistry.* 2008;69(5): 1111-1118.
- [16] Ajayan, P. M., Schadler, L. S. and Braun, P. V. Nanocomposite Science and Technology. Wiley-VCH GmbH & Co. KGaA. ISBN 3-527-30359-6, 2003.
- [17] Calebrese C et. al. A review on the importance of nanocomposite processing to enhance electrical insulation. *IEEE Trans. Dielectr. Electr. Insul.* 2011; 18: 938.
- [18] Zhou K et al. Dielectric response and tunability of a dielectric-paraelectric composite. *Appl. Phys. Lett.* 2008;93: 102908-102911.
- [19] Ismail H et al. Properties of ferrite-filled natural rubber composites. *Polym. Plast. Technol. Eng.* 2007;46: 641-650.
- [20] Spaldin NA. Magnetic materials: Fundamentals and device applications. Cambridge University Press; 2003.
- [21] Malini KA et al. Magnetic and processability studies on rubber ferrite composite based on natural rubber and mixed ferrite. *J. Mater. Sci.* 2001;36: 5551.
- [22] Daigle A et al. Structure, morphology and magnetic properties of  $\text{Mg}_{(x)}\text{Zn}_{(1-x)}\text{Fe}_2\text{O}_4$  ferrites prepared by polyol and aqueous co-precipitation methods: a low-toxicity alternative to  $\text{Ni}_{(x)}\text{Zn}_{(1-x)}\text{Fe}_2\text{O}_4$  ferrites. *Nanotechnol.* 2011;22(30): 305708.
- [23] Feldman C. Polyol-mediated synthesis of nanoscale functional materials. *Solid State Sci.* 2005;7: 868-873.

- [24] Nobre MAL. Varistores a Base de ZnO Obtidos a Partir das Fases  $\text{ZnSb}_2\text{O}_6$  e  $\text{Zn}_7\text{Sb}_2\text{O}_{12}$ : Correlação entre as Fases, Microestrutura e Propriedades Elétricas. PhD thesis. Universidade Federal de São Carlos; 1999.
- [25] Grison EC, Hoinacki E, Mello JB. Curso de tecnologia da borracha. Associação Brasileira de Química; 1984.
- [26] Bellucci FS et al. Método de produção de nanocompósitos funcionais e produtos obtidos. Patent filing n° BR102012005278-4, 2012, international extension n° PCT/BR 2013/000063; 2013.
- [27] Bellucci FS et al. Mechanical Properties of Vulcanized Natural Rubber Nanocomposites Containing Functional Ceramic Nanoparticles. *Sci. Adv. Mater.* 2013;5: 637.
- [28] Rodriguez-Carvajal J. FullProf: A Program for Rietveld refinement and Pattern Matching Analysis. Collected Abstracts of Powder Diffraction Meeting, Toulouse, France, 1990;127.
- [29] CPDS: Diffraction Data Base. Newton Square: International for Diffraction Data, CD-ROM, 1999.
- [30] Moraes J et al. *Schistosoma mansoni*: In vitro schistosomicidal activity of pipartine. *Exp. Parasitol.* 2011;127: 357-364.
- [31] Bellucci FS. Caracterização dielétrica de partículas nanométricas e nanoestruturadas de óxido de niobato da família tetragonal tungstênio bronze com estequiometria  $\text{KSr}_2\text{Nb}_5\text{O}_{15}$ . MSc dissertation. Univ Estadual Paulista; 2008.
- [32] Lanfredi S, Cardoso CX, Nobre MAL. Crystallographic properties of  $\text{KSr}_2\text{Nb}_5\text{O}_{15}$ . *Mater. Sci. Eng., B.* 2004;112: 139-143.
- [33] Ma R et al. Synthesis, characterization and electromagnetic studies on nanocrystalline nickel-zinc ferrite by polyacrylamide gel. *J. Mater. Sci. Technol.* 2008;24: 419-422.
- [34] Desmond KW, Weeks ER. Random close packing of disks and spheres in confined geometries. *Phys. Rev. E.* 2009;80: 051305.
- [35] Jamal EMA et al. On the magnetic, mechanical and rheological properties of rubber-nickel nanocomposites. *Polym. Bull.* 2010;64: 907.
- [36] Lanfredi S. Thermistor behaviour and electricconduction analysis of Ni-doped niobate ferroelectric: the role of multiple  $\beta$  parameters. *J. Phys. D: Appl. Phys.* 2012;45: 435302.
- [37] Ma R et al. Synthesis, characterization and electromagnetic studies on nanocrystalline nickel-zinc ferrite by polyacrylamide gel. *J. Mater. Sci. Technol.* 2008;24: 419.
- [38] Trabelsi S, Albouy PA, Rault J. Stress-induced crystallization around a crack tip in natural rubber. *Macromolecules.* 2002;35: 10054-10061.
- [39] Ozbas B et al. Strain-induced crystallization and mechanical properties of functionalized graphene sheet-filled natural rubber. *J. Polym. Sci., Part B: Polym. Phys.* 2012;50: 718-723.



- [40] Departamento de Ciência e Tecnologia, Secretaria de Ciência, Tecnologia e Insumos Estratégicos, Ministério da Saúde. Doenças negligenciadas: Estratégias do Ministério da Saúde. Rev. Saúde Pública. 2010;44: 200.
- [41] Ferreira M et al. Angiogenic properties of natural rubber latex biomembranes and the serum fraction of *Hevea Brasiliensis*. Braz. J. Phys. 2009;39(3): 564-569.
- [42] Bellucci FS. Preparação e caracterização de nanocompósitos multifuncionais obtidos com nanopartículas ferroelétricas e paramagnéticas em filmes de borracha natural. PhD thesis. Univ Estadual Paulista and Universidad de Valladolid; 2013.
- [43] Devorak G, Rovid-Spickler A, Roth JA. Handbook for zoonotic diseases of companion animals Interaction effects on the coercivity and fluctuation field in granular powder magnetic systems. Bayer Healthcare Animal Health; 2008.
- [44] Barboza-Filho CG et al. The influence of natural rubber/Au nanoparticle membranes on the physiology of *Leishmania brasiliensis*. Exp. Parasitol. 2012;130: 152-158.